ACACIA

Advancing the Science for Aviation and Climate

ACACIA

Deliverable 1.1

Title: Report on the observational climatology of cloud-active aviation aerosol, including ice nucleating abilities of contrail processed INPs

Lead partner: ETH Zürich

Project no.	875036
Instrument	Research and Innovation Action (RIA)
Thematic Priority:	H2020-MG-2018-2019-2020
Start date of project:	1 January 2020
Duration:	42 months
Date of report:	30 / 06 / 2020
Document authors:	Zamin Kanji, Andreas Petzold, Baptiste Testa, Christoph Mahnke
Classification:	PU (Public)
File name:	ACACIA-Deliverable D1.1.docx

TABLE OF CONTENTS

1 Introduction

Global civil aviation contributes to anthropogenic climate change via a complex set of processes which are driven by the aircraft gas turbine emissions of carbon dioxide (CO_2), nitrogen oxides (NO_x), water vapour, carbonaceous and sulphate aerosols, and a complex mixture of gaseous hydrocarbon (HC) compounds. An overview of the current state of knowledge about the contributions of civil aviation to climate change is given by Lee et al., (2021). In the context of this deliverable, the particulate matter emissions, and their ability to form ice clouds are of particular interest since they have a strong influence on the climate impact of aviation on cirrus clouds (Burkhardt et al., 2018; Kärcher, 2018).

Aircraft gas turbine engines emit ultrafine particles with diameters below 100 nm, produced by the combustion of hydrocarbon fuels. The emitted aerosol consists of primary carbonaceous particles (composed of black carbon (BC) and organic carbon (OC), also referred to as soot; see Petzold et al. (2013) for details of the used terminology) which are forming in the incomplete combustion process, and of condensation particles nucleating and condensing in the cooling exhaust gas from gaseous precursors, namely sulphuric acid and hydrocarbon vapours (see e.g. Petzold et al. 2005a for an overview). According to their thermal stability, the emitted aerosol particles are classified into two groups: non-volatile (which remain stable at temperatures above 250°C) and volatile (which evaporate below 250°C). The non-volatile mode refers to the carbonaceous particles from fuel combustion, whereas the volatile mode includes droplets composed of sulphur and organic compounds.

The fraction of primary carbonaceous particles is characterised by one particle mode centred at a particle diameter of 25 nm, and a second much weaker mode centred at 150 nm in diameter (Petzold et al., 1999). The number of emitted particles per amount of fuel burned depends strongly on the aircraft engine technology and has been reduced by about one order of magnitude from 1960's technology (2×10^{15} particles per kg fuel) to today's engine technology (less than 4×10^{14} particles per kg fuel); see Petzold et al. (2003).

The volatile mode is characterised by a modal diameter around 10 nm, depending on the age of the exhaust plume. Its formation strength is determined by the fuel sulphur content. One fundamental difference between sulphuric acid based volatile particles and aircraft soot particles is the ability of volatile particles to grow by condensation of gaseous compounds in the early phase of the exhaust plume. In contrast, aviation soot particles remain at the same size; see Figure 1, right panel. Detailed studies by research aircraft at cruising altitude showed that the growth of volatile particles continues up to a plume age of 10 s (Schröder et al., 2000).

Figure 1 illustrates the composition of the aircraft exhaust aerosol (left) and shows measurements at cruise altitude immediately downstream the emitting aircraft.

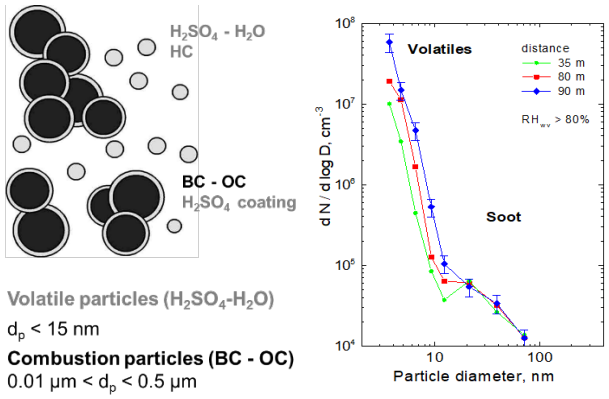

Figure 1: Left: Schematic of aircraft engine exhaust aerosol; adapted from Petzold et al. (2005a). Right: Aircraft exhaust aerosol sampled at cruise altitude close to the emitting engine (distance < 100m); adapted from Schröder et al. (2000).

The interaction of volatile and non-volatile particles by coagulation during the early phase of the aircraft exhaust plume may establish a sulphuric-acid coating on the otherwise hydrophobic aviation soot particles. Detailed studies on aircraft soot proved the strong increase in the ability of soot particle to serve as cloud condensation nuclei as a function of sulphuric acid coating (Petzold et al., 2005b). Whereas the cloud condensation nuclei potential of aviation soot is relevant for the formation of ice crystals in contrails but not in cirrus clouds, a corresponding process with respect to ice nuclei activation is unclear. Nevertheless, aggregated aviation soot particles were found in contrail ice crystals at an enriched level compared to natural cirrus (Petzold et al., 1998). One question we seek to address in this work package is what is the fate of these aggregated aviation soot particles that are released into the cirrus environment after contrails have dissipated via sublimation? We seek to investigate their physicochemical properties after contrail activation and their role in cirrus cloud formation.

Aircrafts operate mainly in the upper troposphere/lower stratosphere, altitudes at which cirrus clouds form (Lee et al., 2009). In the cirrus regime, ice crystals can form via homogeneous freezing of aqueous solution droplets if the T < -38 °C and relative humidity over ice (RH_i) is ≥ 140 %. At lower relative humidity, ice crystals can from via heterogenous freezing, through vapor directly depositing as ice onto the surface of solid particles or via a pore condensation and freezing mechanism (see section 3) where liquid water condenses in particle surface pores at RH_i < 140%, freezes in the pore if the temperature

is sufficiently low and subsequently grows out of the pore to form an ice crystal. These solid particles act as ice crystal nuclei and are referred as ice nucleating particles (INPs; Vali et al. 2015). Example of INPs present in the upper troposphere are mineral dust (e.g., Murray et al., 2012 and reference therein). The prerequisites for aerosol particles to nucleate ice are still not fully understood, but it is thought that ice clusters form preferentially on specific surface sites where the energy barrier for ice nucleation is lowered (Kanji et al., 2017); in other words, ice nucleation can occur at warmer temperatures and lower RH_i compared to homogenous freezing if aerosol particles contain these active sites.

From the 1990's and especially in the recent years, many efforts have been devoted to the investigation of the ice nucleating abilities of soot particles (DeMott et al., 1990, 1999; Kanji et al., 2020; Mahrt et al., 2018, 2020a, b; Möhler et al. 2005a, b; Nichman et al., 2019; Popovicheva et al. 2004, 2008; Suzanne et al., 2003). The results are sparse and depend highly on the type of soot and size of the particles investigated. However, soot particles are now thought to be inefficient at nucleating ice above the homogeneous freezing temperature of -38 °C (Kanji et al., 2020) but thought to nucleate ice through pore condensation and freezing where water condensed in soot cavities and confinements (pores) freezes homogeneously at conditions below -38 °C but also RH_i << 140%. The above experiments have been conducted with a variety of soot samples covering a wide range of physicochemical properties. However, experiments with turbine engine soot have not thus far been conducted. Given the wide range of soot properties used, we believe and hypothesize that aviation soot particles are ineffective INPs in the mixed-phase cloud regime (i.e. for T > -38 °C), but might act as INPs in the cirrus regime as has been suggested from some of the above mentioned studies that have used proxies of aviation soot.

The relevant properties for soot particles to act as INPs in the cirrus regime are the morphology and mixing state (see section 3.1.2). They both depend on the soot emission source and vary greatly from wildfire to diesel or aircraft engine emission (Vander et al., 2010; Wentzel et al., 2003). Moreover, changes on the morphology and mixing state can occur beyond emissions through several aging processes such as surface oxidation, organic and/or inorganic coating or cloud processing (e.g., Mahrt et al. 2020a, b; China et al., 2015; Friebel et al. 2019; Zhang et al. 2020). However, the impact of atmospheric soot aging on their ice nucleating abilities is still unclear. Furthermore, the ice nucleating ability of real aircraft soot has not been investigated so far and are thought to be different to commercial and lab-generated soot particles, such as those investigated in past studies.

In recent publications, and also in the context of ACACIA, the magnitude of the climate effect of aviation soot is investigated, and there are valuable arguments that this effect is small if aviation soot particles are very inefficient ice nucleating particles (Kärcher et al., 2021; Righi et al., 2021). In that respect, both the state-of-the-art knowledge on the occurrence of aviation soot in at cruising altitude (Chapter 2) and new knowledge on the ice nucleating ability of real aircraft engine exhaust particles (Chapter 3) are of paramount importance for an improved understanding of the climate impact of aviation.

2 Observational climatology of aviation aerosol

This section describes the aviation aerosol climatology extracted from IAGOS-CARIBIC data and first analyses based on these data.

2.1 Methods used to identify aviation aerosol within the IAGOS-CARIBIC data and aerosol parameters determined from each aviation aerosol plume

To be able to set up an observational climatology of aviation aerosol it is crucial to first identify the aircraft exhaust plumes. This section describes the method used to identify aviation aerosol by

identifying the time periods during which the IAGOS-CARIBIC flying laboratory was measuring within aircraft exhaust plumes. Furthermore, we describe the methodology how each individual detected aviation plume is analysed and which aerosol parameters, trace gas parameters, and other atmospheric parameters were determined for them.

2.1.1 Aircraft plume detection algorithm

The basic principle used for the detection of aircraft exhaust plumes is to search for a simultaneous enhancement of multiple aviation fuel combustion products like the total aerosol particle number (concentration or mixing ratio) and the mixing ratio of the total reactive nitrogen (NO_y), which are used here. A visualisation of this principle is shown in Figure 2.

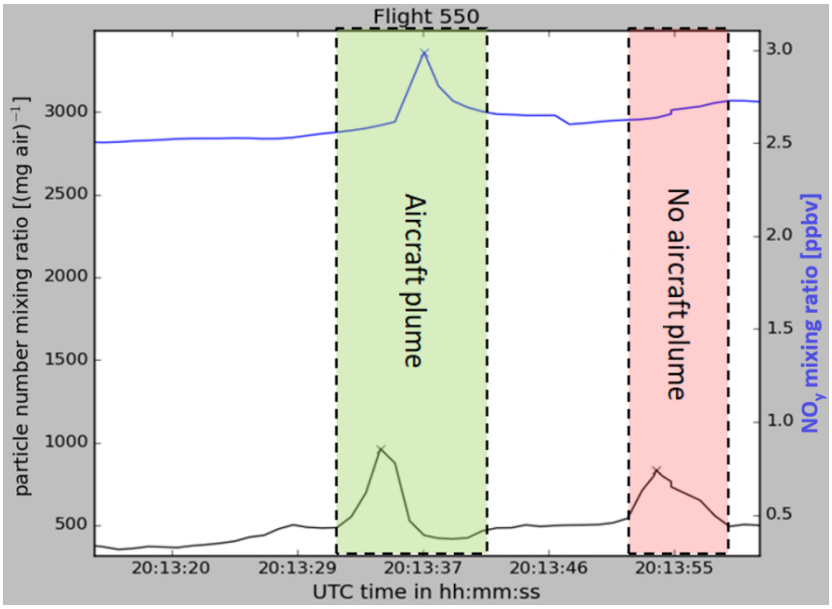

Figure 2: Plume detection principle

Additionally, the used measurement data must have a high temporal resolution. This is necessary to be able to resolve the short encounters with the aircraft plumes, which are typically only a few seconds long. Because we are searching for a simultaneous enhancement of two species, the measurements must also be synchronized as precise as possible.

The IAGOS-CARIBIC flying laboratory contains the IAGOS-CORE aerosol instrument (Bundke et al., 2015a), which measures multiple aerosol particle parameters (see also Table 1) with 1 Hz temporal resolution and also the NO_y measurements by the DLR on IAGOS-CARIBIC (Stratmann et al., 2016a) are provided with 1 Hz temporal resolution.

To be able to detect as many aircraft plumes as possible within a big data set, like the one provided by the IAGOS-CARIBIC flying laboratory, a Python based automated plume detection algorithm was developed. This algorithm searches for peaks within the time series of the aerosol particle number mixing ratio (for particle diameters > 15 nm) and the NO_y mixing ratio. For each of the two species the peak detection was set up individually to avoid artefacts due to peaks which are e.g. to broad to be a potential aircraft plume. In a next step the algorithm matches simultaneous occurring peaks between the two species. Figure 3a shows an example how well this matching works for synchronized datasets. But, as the synchronization was not perfect in all cases, the matching algorithm allowed a time-shift between the peaks. This means, for two peaks to be matched, the aerosol and NO_y peak limits must overlap. To avoid mismatches, for bigger time-shifts (see Figure 3b) the peaks are not matched as aircraft plumes. Multiple peak matches (shown in the red box in Figure 3c) were removed from the

climatology. These peaks might possibly be multiple overlaying aircraft plumes, but it is not possible to distinguish between them to perform profound further analysis. For this reason, the observational climatology only includes the data for unique aircraft plumes.

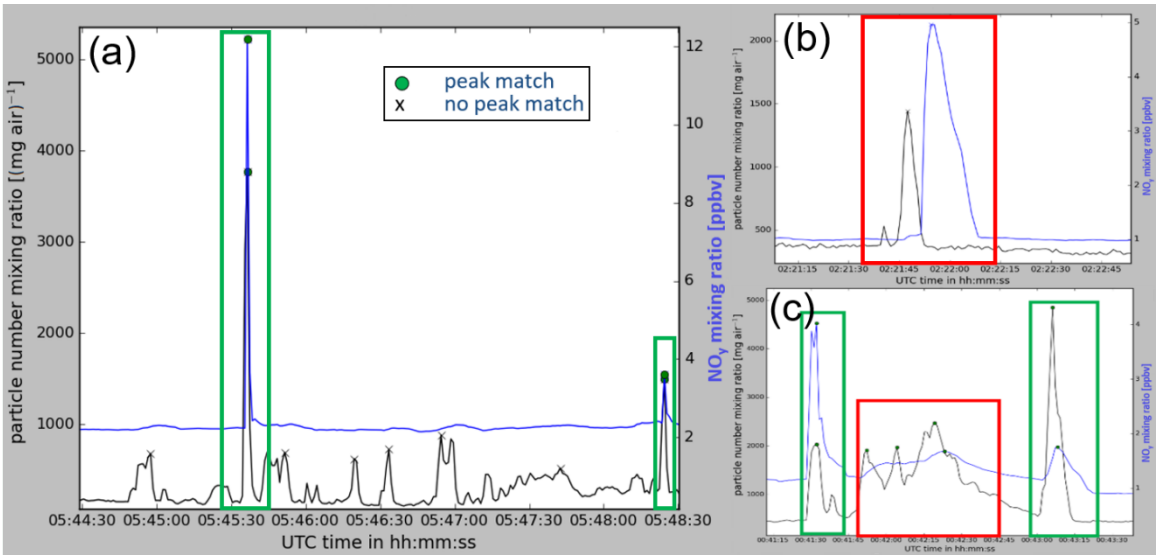

Figure 3: Example cases for the automated peak detection and matching: (a) well synchronized data with matched unique aircraft plumes (green boxes); (b) non matched peaks due to a bigger time-shift; (c) unique detected aircraft plumes (green boxes) and multiple matched peaks (red box).

2.1.2 Individual plume analysis

As a next step, for some parameters, like the total aerosol particle mixing ratio and the NO_y mixing ratio (see the detailed parameter list in section 2.1.3), not only the mean value for the respective parameter, but also the individual plume background was calculated within a window around each peak (see red lines in Figure 4). Then, each plume's individual mean excess for the respective parameter was calculated by subtracting the plume's individual mean background from the plume's total mean value. The plumes excess is thereby describing the additional contribution from the aircraft's exhaust to the background within an aircraft plume. Artefacts due to time-shifts between the parameters were avoided by using the peaks width/time information based on the previous peak detection from the individual parameters. This is shown in Figure 4 for an example aircraft plume with the total aerosol particle mixing ratio and the NO_y mixing ratio.

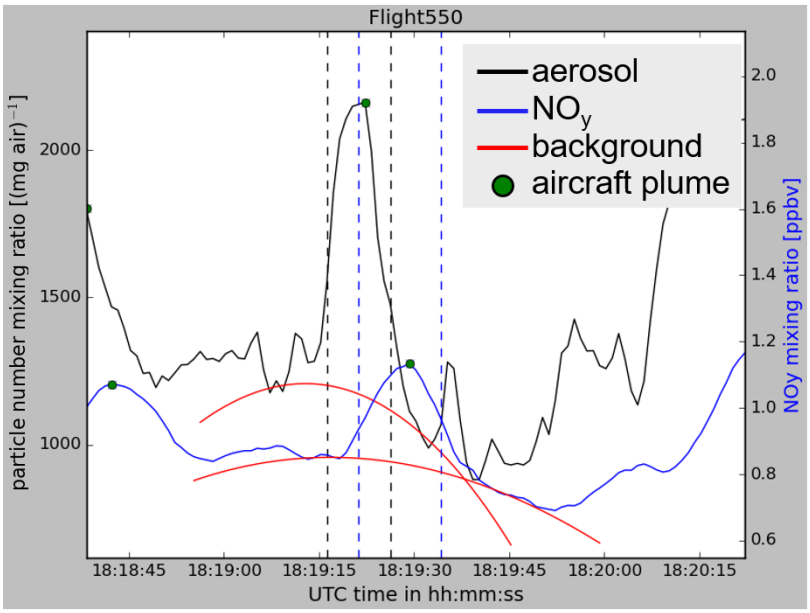

Figure 4: Example visualisation of the automated individual plume analysis: For the total particle number mixing ratio (black line) and the NO_y mixing ratio (blue line). The black and blue vertical dotted lines represent the individual peak width respectively. The individually determined background within a window around the peak of each parameter is marked with the red lines. The green dots indicate that these peaks belong to a matched unique aircraft plume.

2.1.3 Aerosol, trace gas and other atmospheric parameters determined for each aviation plume

With the automated aircraft plume detection and analysis (see sections 2.1.1 and 2.1.2), each plume's individual excess and background mean values, peak maximum value, peak width as well as the timestamps for each peak start, peak maximum, and peak end were calculated for all aerosol particle parameters listed in Table 1, and also for the NO_y mixing ratio. For O_3, NO, and CO (CO is not available for all flights / aircraft plumes) the total mean values were calculated for the individual plumes.

parameter	units	property
total aerosol particles (number concentration and particle mixing ratio)	$(mg\ air)^{-1}$, cm^{-3}	total number of emitted particles with diameter > 15 nm, including non-volatile combustion particles and volatile secondary particles
non-volatile aerosol particles (number concentration and particle mixing ratio)	$(mg\ air)^{-1}$, cm^{-3}	number of emitted combustion particles containing a carbonaceous core, with particle diameter > 15 nm, after being heated up to 250 °C in a thermal denuder
accumulation mode particles (number concentration and particle mixing ratio)	$(mg\ air)^{-1}$, cm^{-3}	number of large particles with particle diameter > 250 nm
non-volatile aerosol fraction		fraction of combustion particles (particle diameter > 15 nm, after being heated up to 250 °C in a thermal denuder)
accumulation mode / total aerosol fraction		fraction of large particles with particle diameter > 250 nm

Table 1: Available aerosol parameters measured by the IAGOS-CORE aerosol instrument integrated in the IAGOS-CARIBIC flying laboratory (Bundke et al., 2015a).

For the additional atmospheric and geographic parameters (listed in Table 2) the mean value for each individual aircraft plume was calculated.

parameter	units
barometric altitude	m
longitude	degree
latitude	degree
static temperature	K
potential temperature	K
static pressure	hPa
pressure level relative to the thermal tropopause	hPa
total water (volume mixing ratio) *	ppmv
gas phase water (volume mixing ratio) *	ppmv
relative humidity over ice *	%

Table 2: List of additional available atmospheric and geographic parameters. *: This parameter is not available for all aircraft plumes.

2.2 Description of the aviation aerosol climatology in terms of the classification of the detected aviation plumes

The aviation aerosol climatology contains the data for 1135 unique aviation exhaust plumes. These plumes were encountered during 36 of the 42 flights conducted by the IAGOS-CARIBIC flying laboratory between 29 July 2018 and 4 March 2020. This section describes this climatology in terms of the global and seasonal distribution of its containing aviation plume data, as well as the classification between their tropospheric or stratospheric characteristics, and if they were measured under clear-sky or in-cloud conditions.

2.2.1 Geographical distribution

Because the IAGOS-CARIBIC flying laboratory is integrated aboard an in-service Lufthansa airliner, the here discussed measurements were conducted within the main flight corridors between the aircraft's base airport in Munich (Germany) and destinations in North America, East Asia, and South Africa.

Figure 5 shows the global map with the analysed IAGOS-CARIBIC flights (flight tracks marked as blue lines) and the detected unique aircraft plumes (marked as red dots).

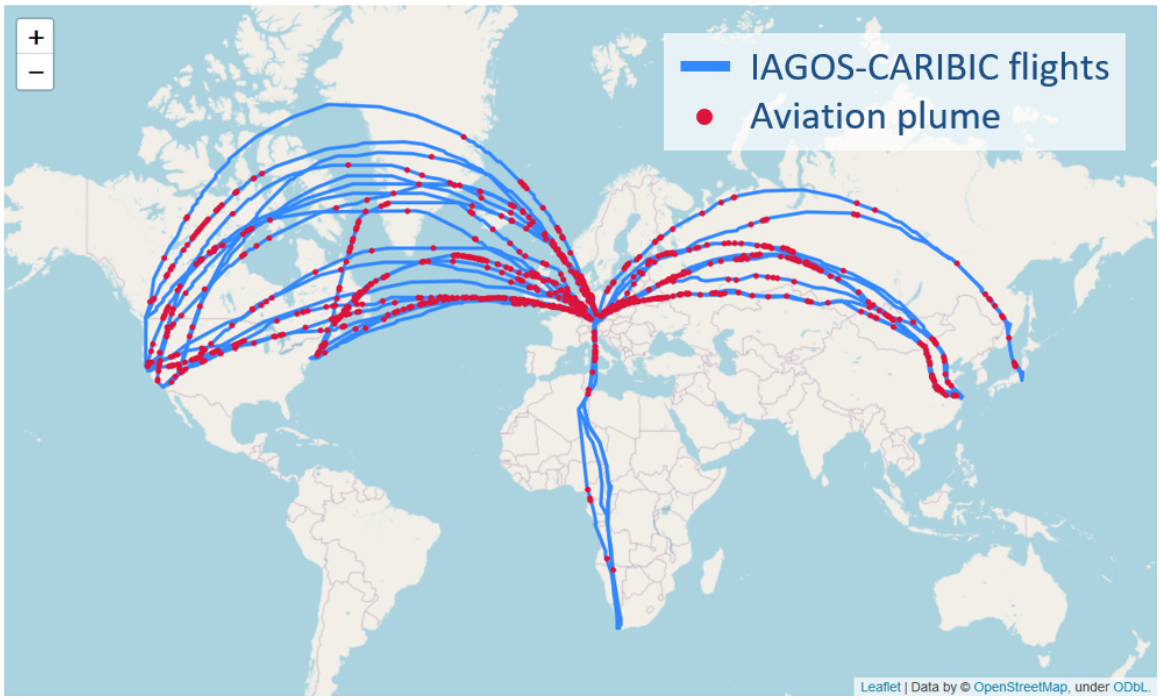

Figure 5: Global map with all analysed IAGOS-CARIBIC flights. Flight tracks represented by blue lines and all detected unique aviation plumes marked with red dots.

2.2.2 Tropospheric/stratospheric characteristics

The aircraft plumes were vertically classified by their individual tropospheric/stratospheric characteristics. For this purpose, the mean pressure level relative to the thermal tropopause (Δp_{trop}) was calculated for each encountered aircraft plume. The strong increase of the ozone mixing ratio (mean values for each individual aircraft plume) at the thermal tropopause, shown in the right panel of Figure 6, confirms the agreement of the thermal tropopause hight (based on the operational ECMWF analysis data) with the observed chemical tropopause. A histogram analysis for all plume mean values of Δp_{trop}, with Δp_{trop} as the vertical coordinate is shown in the left panel of Figure 6. Of all 1035 detected aircraft plumes, 720 (63%) were stratospheric ($\Delta p_{trop} < 0$) and 415 (37%) tropospheric ($\Delta p_{trop} > 0$). With in total 1015 (89%), most of the aircraft plumes were observed within a relative pressure distance of ± 100 hPa around the thermal tropopause (-100 hPa < Δp_{trop} < 100 hPa).

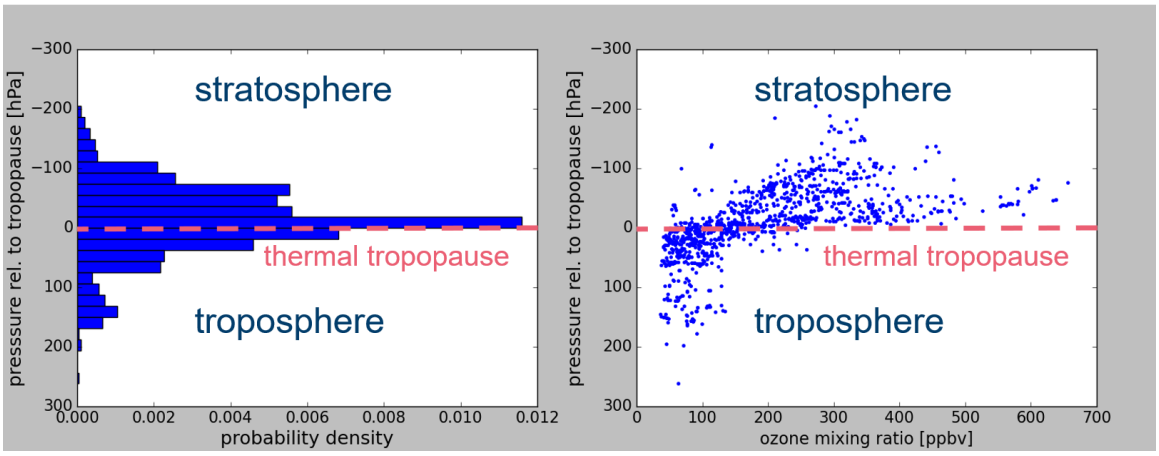

Figure 6: Left panel: Histogram analysis of the pressure level relative to the thermal tropopause for all detected aircraft plumes. Right panel: Vertical profile of the mean ozone mixing ratio for each aircraft plume with the pressure level relative to the thermal tropopause as vertical coordinate.

2.2.3 Clear sky or in-cloud conditions

Furthermore, the detected aircraft plumes were classified by their occurrence under clear sky or in-cloud conditions. For this purpose, the difference between total and gas phase water measurements was used. This information is available for 488 of the 1135 detected aircraft plumes. Of these 488 plumes 58 (12%) were observed under in-cloud and 430 (88%) under clear sky conditions. An additional seasonal classification of this information is shown in Table 3.

2.2.4 Seasonal distribution

Aviation aerosol related atmospheric processes like the formation of contrail cirrus and its radiative forcing (Kärcher, 2018), photochemical heterogeneous reactions, and atmospheric transport have a seasonal dependency. Table 3Table 3 shows the statistical basis for the analysis of this seasonal processes for all detected aircraft plumes as well as further classified by their tropospheric/stratospheric and clear sky/in-cloud characteristics.

Season	total a/c plumes	tropospheric	stratospheric	clear sky *	in-cloud *
Dec-Feb	200	62	138	116	21
Mar-May	48	20	28	40	8
Jun-Aug	513	251	262	145	20
Sep-Nov	374	82	292	129	9

Table 3: Seasonal distribution of the observed aircraft plumes. *: This information is only available for 488 of the 1135 detected aircraft plumes.

2.3 First analysis based on the aviation aerosol climatology

The previously described aviation aerosol climatology, with its 1135 unique aircraft plumes, provides a solid basis for statistical analysis of the atmospheric aviation aerosol. In this section we present first statistical analysis of the aviation aerosol's properties in terms of number, size, and volatility.

2.3.1 The aerosol particle number mixing ratio

First, we look at the impact of the aviation aerosol on the total and the accumulation mode aerosol number mixing ratio in relation to their atmospheric background values. For this a histogram analysis over all 1135 aircraft plumes was done for the excess aerosol particle number mixing ratio and the background. For the background all data points from the analysed flights were used, after the detected aircraft plumes were removed from the data set. To account for the averaging over the individual plumes, the 1 Hz resolved background data set was averaged with a 10-seconds running mean. Figure 7 shows this analysis for the total aerosol (diameters > 15 nm; left panel) and for the accumulation mode particles (diameters > 250 nm; right panel).

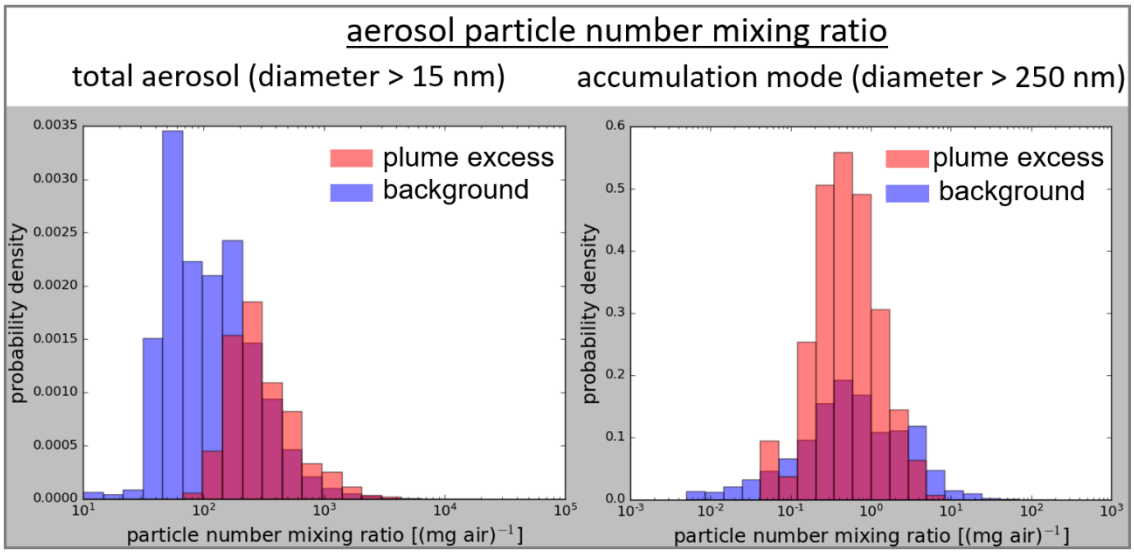

Figure 7: Histogram analysis of the aerosol particle number mixing ratio of the plumes excess and the background for particles with diameters > 15 nm (left panel) and diameters > 250 nm (right panel).

As a next step the same histogram analysis was applied to the accumulation mode fraction (accumulation mode particle number mixing ratio normalized by the total aerosol particle number mixing ratio; see Figure 8). Here we see a peak at higher values for the plume excess compared to the overall background. This implies that more larger particles, with diameters > 250 nm like soot, were observed within the aircraft plume compared to the background aerosol.

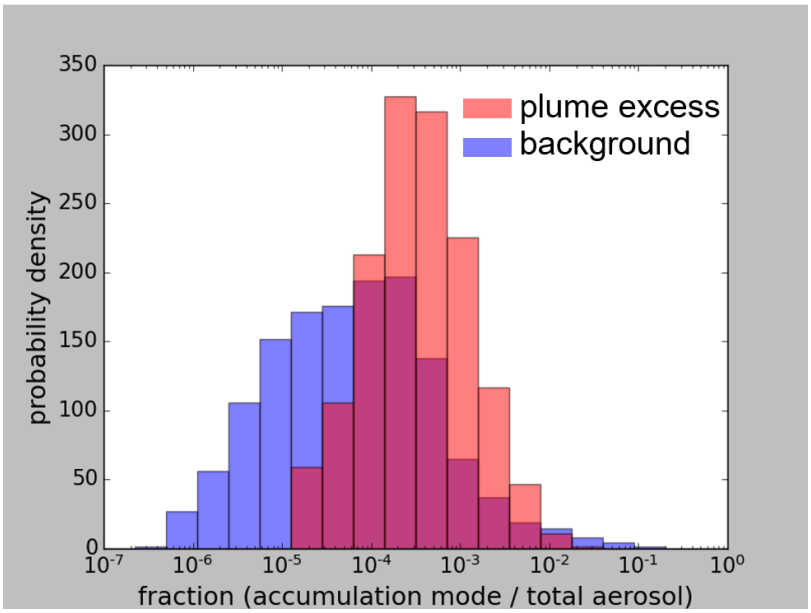

Figure 8: Histogram analysis of the fraction of the accumulation mode particle mixing ratio (diameter > 250 nm) normalized by the total aerosol particle mixing ratio (diameter > 15 nm) of the plume excess aerosol (red) and the background aerosol (blue).

2.3.2 The non-volatile aerosol

To get an information about the mixing state of the observed aviation aerosol, the same histogram analysis principle described in section 2.3.1 was used for the non-volatile aerosol particle number mixing ratio (see right panel of Figure 9) and also for the non-volatile aerosol fraction (see Figure 10). The histogram of the non-volatile aerosol fraction peaks between 0.2 and 0.4 for aircraft plumes

compared to 0.8 for the background. This means that even "aged" plume aerosol shows separate modes of soot (non-volatile) and sulphuric acid (volatile) particles.

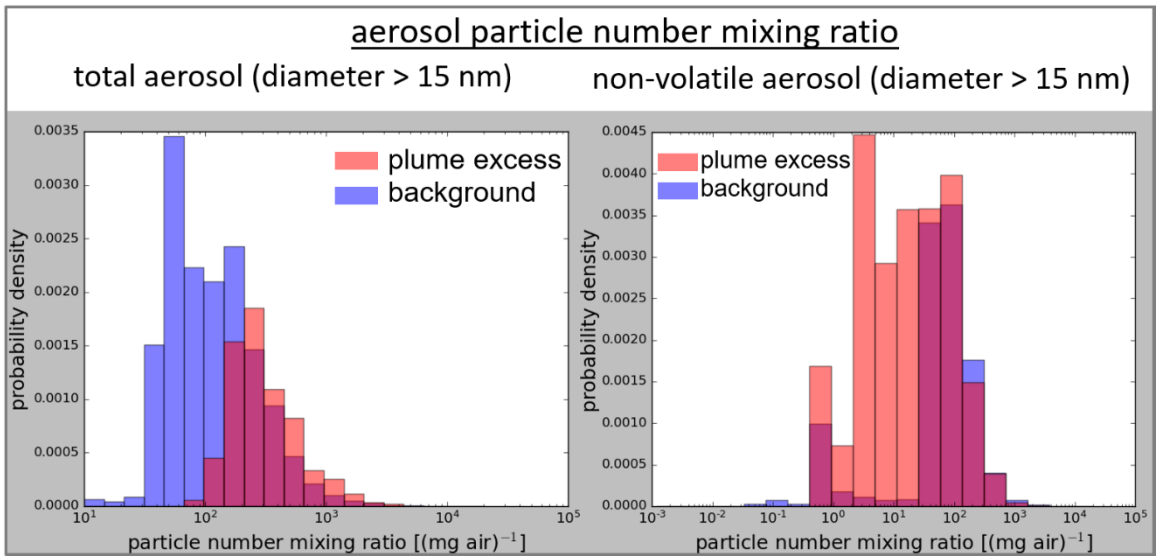

Figure 9: Histogram analysis of the aerosol particle number mixing ratio of the plumes excess and the background for particles with diameters > 15 nm; left panel: total aerosol; right panel: non-volatile aerosol.

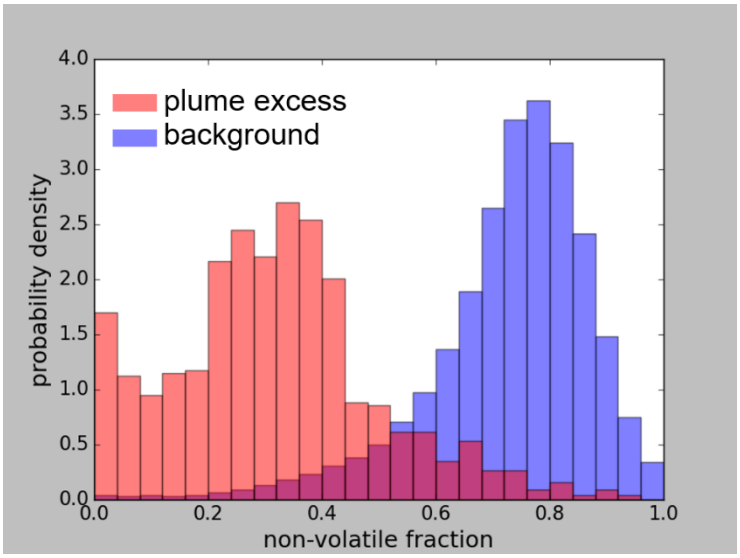

Figure 10: Histogram analysis of the non-volatile fraction of the plume excess aerosol (red) and the background aerosol (blue).

The non-volatile fraction of the aircraft plume excess aerosol as a function of its particle number mixing ratio (for particle diameter > 15 nm) shows no dependence (see Figure 11). This indicates that for the observed plume ages (by means of the range of the excess particle number mixing ratio) no further aging in terms of internal mixing of the aviation aerosol can be observed.

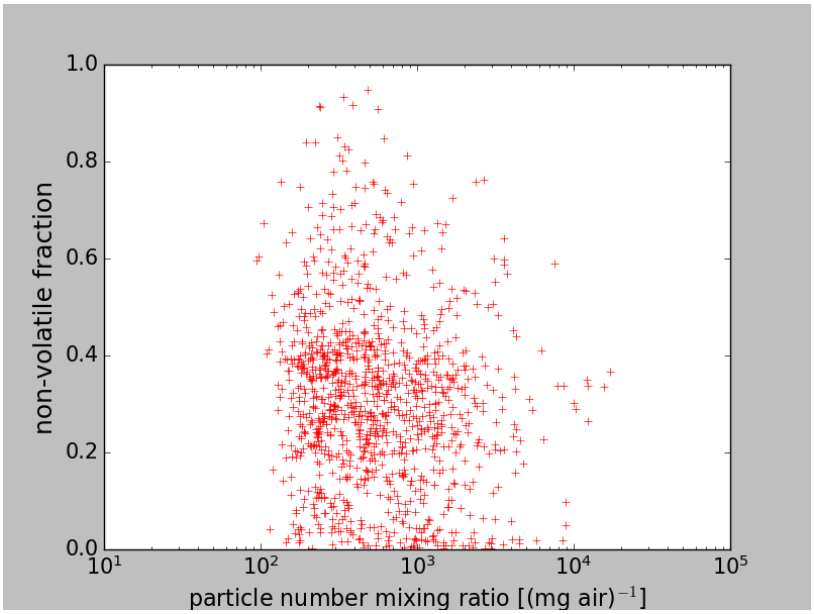

Figure 11: Scatter plot of the excess aerosols non-volatile fraction as a function of its particle number mixing ratio (for particle diameter > 15 nm).

This observational climatology of aviation aerosol includes aircraft plumes with a mean NO_y excess mixing ratio ranging from about 100 pptv to about 10 ppbv and mean excess aerosol particle number mixing ratios (for particle diameter > 15 nm) ranging from about 100 to over 10000 (mg air)$^{-1}$.

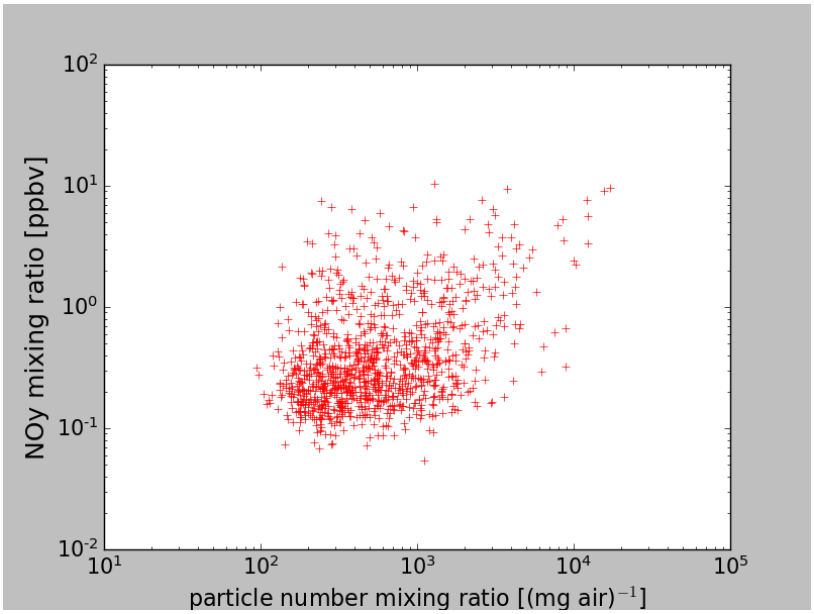

Figure 12: Scatter plot of the excess NO_y mixing ratio as a function of the excess particle number mixing ratio (for particle diameter > 15 nm).

3 Ice nucleating properties of aviation soot

The section aims at presenting 1) state of the art of the abilities of soot particles to form ice crystals and the relevant parameters associated to their ice nucleating abilities (section 3.1), 2) a review of the morphological and mixing state properties of aircraft soot from aircraft measurements and recent/ongoing laboratory studies (section 3.2), and 3) the experimental plan of the ice nucleation measurements of aircraft soot that will be conducted in Oct-Nov 2021 and Apr-May 2022 at the Zürich aircraft turbine facility (section 3.3). We note that this section of the project had a 10-month delay in starting due to the pandemic. As such the first set of measurements with aircraft turbine soot are only planned for fall 2021 as indicated above. However, we have started conducting experiments on proxies of turbine soot to investigate the effect of some ageing processes on cirrus cloud ice nucleation for temperature (T) below -40 °C. The ageing processes include condensation of volatiles like sulphuric acid (H_2SO_4) and ozone (O_3) ageing of soot particles, both processes relevant for aircraft corridors in the upper troposphere.

3.1 Ice nucleation pathway of aircraft soot and relevant parameters

3.1.1 Aircraft soot particles freeze via pore condensation and freezing

There exists substantial evidence of the emission of soot particles by aircraft turbine in the upper troposphere and their implication in the formation of contrail clouds and contrail cirrus clouds (Kärcher, 2018). Nevertheless, only few modelling studies investigated the potential of aircraft soot to promote ice crystal formation after contrail sublimation and to trigger or alter the formation of cirrus cloud (see review study from Lee et al., 2021). The modelling results are sparse and depend highly on the aircraft soot properties and abilities to form ice (Righi et al. 2021). In the recent years, many laboratory studies have been devoted to the ice nucleation mechanism of soot particles (Bhandari et al., 2019; China et al. 2015; Kanji et al., 2020; Mahrt et al. 2018, 2020a, b; Nichman et al., 2019; Ullrich et al., 2017; Zhang et al., 2020). Through the latest literature from 2018 onwards, it is now clear that soot particles can cause ice crystal formation at cirrus relevant conditions (Mahrt et al. 2018, 2020a, b; Nichman et al., 2019) via the pore condensation freezing mechanism through homogeneous freezing of pore water (PCF mechanism, Marcolli 2014, 2020, 2021) for temperatures below -38 °C and below water saturation (i.e. RH_w < 100%; RH_i < 140%), i.e. under conditions where the homogeneous freezing of aqueous solution droplets is irrelevant due to droplet activation. The cavities and slits, formed between soot primary particles, can be seen as pores (see Figure 13, primary particle outlined in blue), where liquid water can condense below water saturation due to the inverse Kelvin effect (Christenson, 2013; Marcolli, 2014). Pore water condenses when the RH_w is high enough for the pore-size and composition (contact angle). If the temperature of the water is sufficiently low such that the homogenous ice nucleation rate is large enough, the water in the pore freezes. For soot particles, Marcolli (2020) showed that for typical pore shapes and sizes, this T threshold is ~ -45 °C. Finally, pore ice must grow out of the confinement by vapor deposition in order to be able to spontaneously grow to ice crystal size (see Figure 13). The pores must be narrow enough and the contact angle between the soot surface and the condensed liquid water ($\vartheta_{s/w}$, measuring the surface wettability) must be < 90° to allow condensation below water saturation. On the other hand, the pore volume and the size of the pore opening must be large enough to contain the critical ice germ growing from the liquid phase and from the vapor phase, respectively. Hence, each of these steps can be limited by either the pore size and/or shape, mainly driven by the soot primary particle size (e.g., its diameter d_{pp}) and the surface properties, namely the contact angle with the soot surface and liquid water or ice ($\vartheta_{s/w,i}$). An additional but implicit condition is that the arrangement of the primary particles in the soot aggregate must allow cavities, i.e. pores, to form between the primary particles. The more the number of pores in a soot aggregate, the higher the probability to find a pore with the right size and shape for PCF to occur at a given T and RH. The number of pores in a soot aggregate is driven by the number of primary particles forming the aggregate (N_{pp}), by d_{pp} and by the level of compaction of the aggregate, which can be represented e.g., by the fractal dimension (D_f) of the soot aggregate. The number of pores in

the aggregate is also related to the aggregate size or diameter often measured as the electrical mobility diameter.

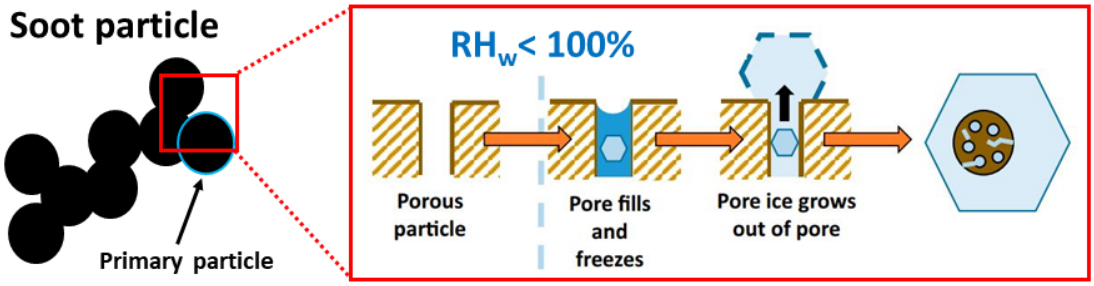

Figure 13: Soot pore freezing leading to ice crystal formation through pore condensation and freezing (PCF) mechanism. Figure adapted from David et al. (2019).

3.1.2 Relevant parameters

Recent studies have shown that commercial soot can freeze via PCF for aggregates ≥ 200 nm; this threshold can vary according to the soot type, i.e. according to their surface and morphological properties (Mahrt et al., 2018: Zhang et al. 2020). Hence, the maximum size of the aircraft turbine soot aggregate is an extremely relevant parameter. Soot aggregates are thought to compact when forming hydrometeors, e.g. ice crystals in contrail clouds, hence increasing the number of pores available for PCF to occur after contrail sublimation, and eventually leading to cirrus cloud formation (Bhandari et al., 2019; Mahrt et al., 2020a). We refer to this process as "cloud processing". The compaction might be due to asymmetrical liquid water induced capillary forces on the soot structure during evaporation/sublimation of the ice crystals containing the soot aggregates (China et al., 2015; Ma et al., 2013). However, whether aircraft soot particles can induce freezing at cirrus conditions after cloud processing is not clear (Marcolli, 2021; Mahrt et al. 2020) and will be therefore addressed by a series of *T* and *RH* controlled experiments performed at the Zürich airport with real aircraft turbine soot particles (section 3.3 presents the experiments plan).

The mixing state of soot has proven to influence its ability to form ice. Coating of soot particles with H_2SO_4 showed both increase and decrease of its ice nucleation onset RH_i (DeMott et al., 1999; Möhler et al., 2005a; Mahrt et al. 2020b). On the one hand, directly condensed H_2SO_4 might inhibit PCF due to induced freezing temperature depression in the pores (Marcolli, 2014, 2021) but on the other hand, H_2SO_4 adsorbed at the soot surface increases the soot hydrophilicity (i.e., decreases its contact angle; Mahrt et al., 2020b; Popovicheva et al., 2011) thus promoting condensation but also might cause morphological restructuring (Zhang et al., 2008) that promotes pore formation. The affinity of soot particles to H_2SO_4 might depend on the soot properties (e.g., d_{pp} and surface organic content), which will influence how the acid interacts with the soot surface resulting in different ice nucleating abilities. Surface organic content generally decreases the soot ice nucleating abilities (Möhler et al., 2005b; Ullrich et al., 2017; Mahrt et al. 2020b). Surface oxidation is thought to facilitate the uptake of water by the soot particles but has been shown to not necessary lead to enhanced soot freezing behaviour (Nichman et al., 2019 and reference therein). Yet, the relative impact of chemical aging (e.g., coating, surface oxidation) compared to morphological changes (e.g., during cloud processing) on the ice nucleating abilities of aircraft turbine soot particles is not clear and will be also investigated.

3.2 Characterization of aircraft soot properties from (in-situ and ground-based) aircraft and lab studies

3.2.1 Size and morphological characterization

In general, the measurements of d_{pp} of aircraft soot particles converge to values between 10 nm < d_{pp} < 40 nm for in-situ studies (e.g., Petzold et al. 1997, 1998; Posfai et al. 1999) and ground-based studies (Bescond et al. 2014; Delhaye et al. 2017; Liati et al., 2014; Lobo et al. 2015; Moore et al., 2017), with increasing sizes for increasing thrust (Delhaye et al. 2017; Liati et al., 2014; Lobo et al., 2015).

As mentioned above, large soot aggregates are more likely to freeze compared to smaller ones. Ground-based studies have shown that diameter modes of aircraft soot agglomerate range from few primary particles to ~ 80 nm, with few agglomerates up to ~ 120 nm (Liati et al., 2019; Lobo et al. 2015; Popovicheva et al., 2004), consistent with in-situ studies that found most agglomerates below 200 nm (Petzold et al. 1998, 1999, Posfai et al. 1999). However, few studies observed larger agglomerates, e.g. about 400 nm in Twohy and Gandrud (1998), few agglomerates > 560 nm in Twohy and Poellot (2005) (although the aircraft origin of the agglomerates is not certain) and up to 0.8 µm interstitial contrail soot particles with some metallic inclusions in Petzold et al. (1998). The fraction of this large agglomerate is low and might have been biased by the lower detection limit of 100 nm in these studies. Petzold et al. (1998) found soot agglomerates up to 1 µm in contrail ice residuals and argue that such large soot particles might have formed during ice crystal evaporation, where the smaller soot particles deposited at the ice crystal surface would collapse with soot particles within the ice crystals. The large agglomerates of ~ 1 µm are substantially larger than the sizes measured at the ground (up to ~ 100-200 nm). Such large agglomerate might have formed via coagulation of smaller soot cluster in aircraft wing vortices, where the mixing volume are rather small and prior dilution in the jet plume (Miake-Lye et al., 1993). However, measurements of the maximum size of aircraft soot particles and its relative concentration in the jet exhaust plume are still sparse. Nonetheless as part of this work package (section 2, Figure 7) we can see that the fraction of accumulation mode particles (> 250 nm) in aircraft plume are non-negligible compared to the background particle concentration. This could hint at the presence of larger soot particles being present in the aircraft or contrail plumes. But size distribution measurements would be necessary to confirm this.

3.2.2 Mixing state characterization

The effect of jet fuel sulphur content (FSC) on aircraft exhaust particles and contrail properties has been investigated by few studies in the 90's (see review from Schumann et al., 2002). They show that the number of ice crystals in contrail varies from no increase to about 10-fold increase from low to high FSC (~ 3-3000 µg/g), suggesting an enhancement of soot activation as ice crystals, due to H_2SO_4. However, the diversity of the results as well as instrument limitations did not allow robust final conclusions. Although the number of volatile particles was found to increase with increasing FSC (~10-fold increase for a FSC of ~ 3 µg/g to ~ 3000 µg/g), soot properties are thought to be independent on FSC (Schumann et al., 2002). Besides, for low FSC (e.g., ~ 3 µg/g), organic trace gases and oxygen-containing volatile particles are thought to dominate over H_2SO_4 (Schumann et al., 2002). A significant fraction of the volatile particles is deemed to be scavenged by contrail ice crystal, potentially affecting the mixing state of soot particles that remain after contrail sublimation. Current regulations impose a maximum sulphur content of 3000 ppm, although mean FSC is current jet fuel is about 600-800 ppm (reduction of sulphur limits in aviation fuel standards (SULPHUR), Research project EASA.2008/C11). However, information on the mixing state of contrail processed aircraft soot particles and its evolution as the soot particles age, are lacking, but important regarding their nucleating abilities, as mentioned above.

3.2.2.1 Effect of H_2SO_4 coating on soot ice nucleating abilities

A recent study conducted at ETH Zürich (Gao et al. 2021, in preparation) investigates the effect of H_2SO_4 coating on the ice nucleating abilities of miniCast black soot (propane diffusion flame soot, considered as a proxy for aircraft soot; Ess and Vasilatou 2019; Marhaba et al., 2019). Soot particles were injected in a coating apparatus saturated with H_2SO_4 and cooled down to lower temperatures, allowing the condensation of H_2SO_4 onto the particles. The coated soot particles were then exposed to ice-supersaturation conditions at cirrus cloud relevant temperature (T < -40 °C) in a continuous flow diffusion chamber (HINC: Horizontal Ice Nucleation Chamber; see e.g. Lacher et al., 2017), allowing the ice crystals to from. The fraction of soot particles forming ice crystals (activated fraction, ***AF***) as a function of RH_w for uncoated and coated soot with different H_2SO_4 coating mass fractions is shown on Figure 14 left panel for -45 °C. Bare soot starts to freeze at homogeneous freezing RH_w (RH_w^{hom}) and nucleation via PCF is not observed. As RH_w crosses the RH_w^{hom} barrier, a steep increase in the *AF* signal is observed which represents water uptake onto the soot particles followed by homogeneous freezing (droplet freezing). When the soot particles are exposed to a small amount of H_2SO_4 (thin coating, Figure 14 left panel), H_2SO_4 vapor preferentially condenses into the pores (due to inverse Kelvin effect, pore saturating vapor pressure is lower compared to over the soot surface). Partial or complete filling of the pores induces a depression of their freezing temperature (lower water activity compared to pure water; Koop et al., 2000) which would explain the observed delayed onset freezing and lower *AF* compared to bare soot. If the soot particles are exposed to higher H_2SO_4 partial vapor pressure (medium and thick coatings), the soot surface starts to acquire a thin H_2SO_4 coating (10.96 and 28.12 wt% in Figure 14 left panel). As RH_w increases, the soot particles take up more water due to their enhanced hydrophilicity, induced by H_2SO_4 coating, and would behave as liquid H_2SO_4 droplets, which would readily freeze as soon as RH_w^{hom} is reached. Thick H_2SO_4 coatings have been shown to increase the *AF* of organic-rich soot compared to bare uncoated particles (results not shown here). For organic-rich aviation soot, the latter effect might explain the observed enhanced contrail ice crystal number concentration while burning jet fuel with higher FSC (observations reviewed in Schumann et al., 2002). In summary, thin H_2SO_4 coatings inhibits miniCast black soot (organic-poor soot) ice nucleation by inducing a depression of the pore freezing temperature, leading to delayed onset freezing and smaller overall *AF* when only the pores are filled, and to acidic-like droplet freezing abilities, when the soot are partially coated.

3.2.2.2 Effect of O_3 ageing on soot ice nucleating abilities

Another atmospheric relevant soot ageing process is surface oxidation, which is thought to affect the soot chemical surface functionalities and the soot surface nanostructure (i.e., generally resulting in enhanced soot hydrophilicity, Grimonprez et al. 2018; Friebel et al. 2019), potentially leading to change in the soot freezing abilities (Brooks et al., 2014; Lupi and Molinero, 2014). The most effective oxidants in the atmosphere are OH radicals and O_3 (Finlayson-Pitts and Pitts, 1999). Therefore, a series of O_3 ageing experiments of aircraft soot proxies (miniCast brown and black) is ongoing in our laboratory at ETH. Figure 14 right panel shows preliminary ice nucleation results of 200 nm diameter miniCast brown soot particles (organic-rich soot from propane diffusion flame; Moore et al., 2014) aged in O_3 (20ppm at ambient pressure and temperature for ~2.5 min). These experiments were compared to unaged soot particles of the same kind as well as particles that were O_3 aged and contrail processed (T = -45 °C and RH_w = 104 %) before testing for ice nucleation. MiniCast brown soot is an organic-rich soot, making it a good candidate for investigating aging with ozone, as oxidation is thought to be more effective on soot particles with high surface organic content (Browne et al., 2104; Friebel et al., 2019). The blue curve in Figure 13 right panel shows that unaged brown soot freezes homogeneously, meaning that brown soot does not possess the optimal physicochemical properties (pores and contact angle) for PCF. The later freezing and lower activated fraction of the fresh miniCast brown soot compared to miniCast black soot (see black curve in Fig. 14 right panel) is attributed to surface organic species

blocking the pores which renders the surface more hydrophobic or the pores inaccessible to condensation of water (Mahrt et al., 2018). O_3 aged brown soot and aged-cloud processed (red and black curve in Fig. 14 right panel) show some enhancement in ice nucleation activity by activating ice crystals at lower RH_w compared to the blue curve, however we do not consider this to be significant given the overlap in error bars. That being said, the difference between the unaged and the aged-cloud processed is statistically significant. Given that for all three scenarios shown in Figure 14 right panel, the ice crystal activation only occurs at $RH_w > RH_w^{hom}$, this type of soot is not likely to influence cirrus cloud properties, since the background aerosol in the upper troposphere freezes effectively at RH_w^{hom}. The ageing time investigated here (~2.5 min) is very short even though conducted at high O_3 concentrations. This method was used to mimic long ageing times with low O_3 concentrations. However, depending on the mechanism of O_3 reacting with soot surfaces, such a simulation may be too short to fully oxidise the soot particles and could explain why ageing soot with high O_3 concentration shows no effect on their ice nucleating abilities. Therefore, longer aging time (several hours) will be investigated in the next experiments at lower O_3 concentrations (200 ppb) as well as a modified set-up that will allow us to age the soot particles in a *T* and *RH*-controlled environment, thus more representative of real atmospheric aging conditions.

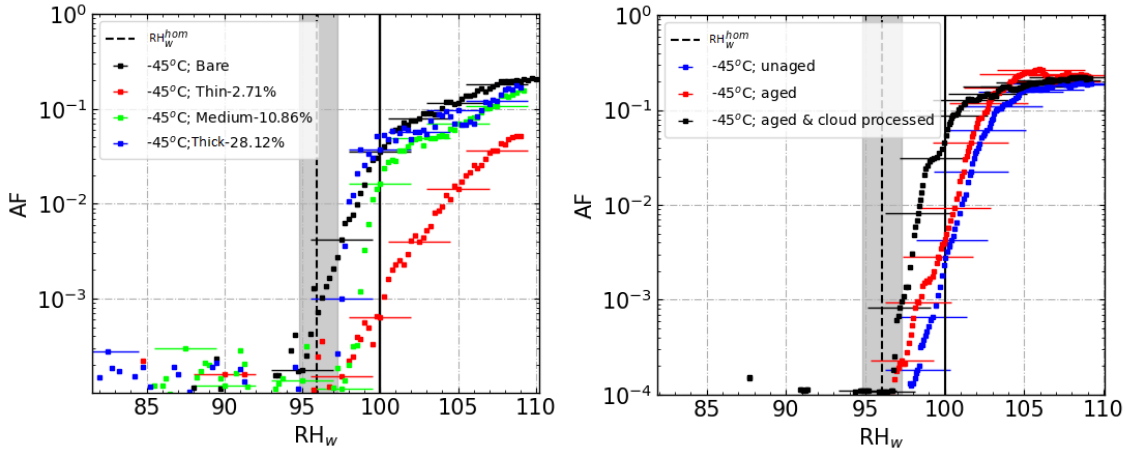

Figure 14: Activated fraction (*AF*) as a function of RH_w. of (left panel) miniCast black soot, bare and coated with different H_2SO_4 coating mass fraction (left panel, percentage values stand for coated H_2SO_4 mass fraction to original particle mass, data: courtesy of Kunfeng Gao) and (right panel) miniCast brown soot, unaged; aged with 20ppm O_3 for ~2.5 min, and aged with 20ppm O_3 for ~2.5 min & cloud processed (at -45°C and RH_w = 104%). O_3 ageing has been conducted at ambient pressure and temperature. Homogeneous freezing lines are computed according to Koop et al. (2000) for a nucleation rate of 1 s^{-1} (assuming 0.5 µm droplet size) ice and liquid water saturating vapor pressures have been computed according to Murphy and Koop (2005).

3.3 Experimental plan

The numerous and recent past studies investigating the ice nucleating abilities of soot have improved our understanding of the freezing mechanism of soot particles, however, these studies used commercial or laboratory soot particles and none conducted ice nucleation measurements of turbine aircraft soot particles so far. Therefore, a series of experiments will be conducted at the aircraft turbine engine facility SMARTEMIS (Swiss Mobile Aircraft Engines Emissions Measurement System) at the Zürich airport, in order to quantify the ability of aviation soot to form ice at cirrus relevant *T* and *RH*, after contrail processing.

A sampling probe will be attached 1.6 m behind the turbine exhaust and will be connected to a heated sampling line, plugged to a 0.3 m^3 stainless-steel reservoir built in-house where soot particles can coagulate. Volatile species will be removed from the turbine exhaust gas with a high flow catalytic stripper (Catalytic Instrument) downstream of the coagulation tank. The particles will then undergo a first cloud in a first ice nucleation chamber, set at contrail conditions. i.e., T < -40 °C and RH_w > 104%

to mimic the cold and highly water vapour supersaturated nature of contrails. After sublimation in a temperature-controlled double-walled jacketed flow tube, the soot ice residuals will be resampled in a second ice nucleation chamber, set at cirrus conditions (-40 °C < T < -55 °C) while ramping from RH_i = ~100% to RH_w slightly >100%. This set-up should mimic cloud processing of aircraft soot by contrail cloud and the subsequent formation of cirrus clouds from cloud processed soot particles. Figure 15 shows the experimental set-up.

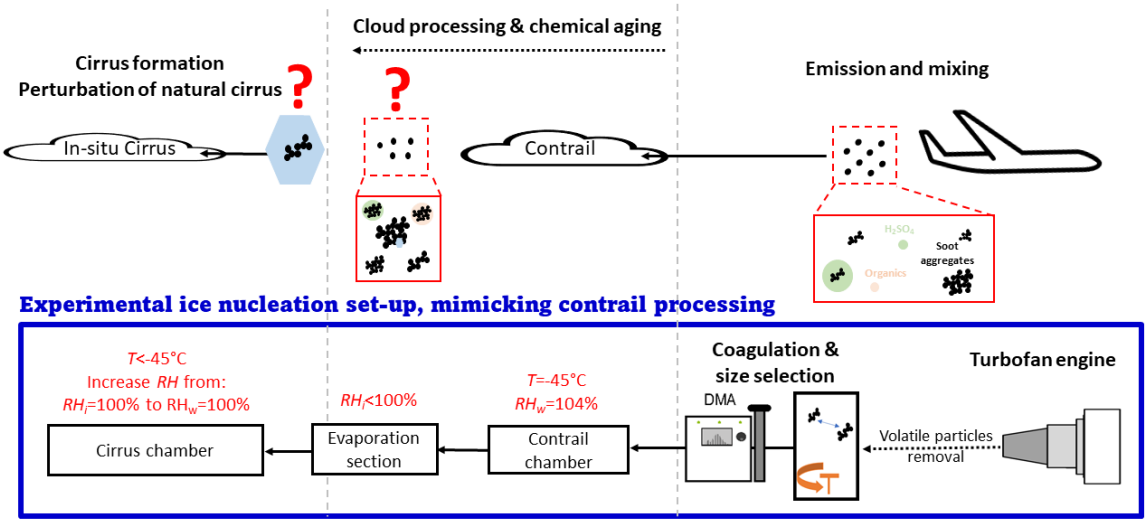

Figure 15: Experimental ice nucleation set-up mimicking the fate of aviation soot particles, from the emission, contrail formation, to cirrus formation/perturbation. See text for more details on the set-up.

A first series of experiments will be performed on unprocessed soot particles (without contrail processing, see experiments 1-5 in table 4), to understand how the ice nucleation properties change (if at all) following cloud processing experiments (experiments 6-11 in table 4).

In addition to the ice nucleation measurements, characterization of the morphology and surface properties of the soot particles will be performed. Shape, d_{pp} and D_f will be inferred from transmission electron microscopy (TEM) images (e.g., Wentzel et al., 2003), soot aggregate sizes with scanning mobility particles sizer (SMPS), mass distribution and D_f with centrifugal particle mass analyser coupled with a differential mobility analyser (DMA-CPMA, see e.g., Mahrt et al. 2018), mixing state with thermal technics (e.g., ThermoGravimetric Analyser) and soot water affinity and pore size distributions with water sorption and gas adsorption methods (e.g., DVS and BET).

Experiment	Soot size	*T* in 1rst chamber	RH_w in 1rst chamber	T/*RH* in sublimation section	*T* in 2nd chamber	*RH* in 2nd chamber	Flight condition	Catalytic Stripper
1. UN ; 400nm	400 nm	--	--	--	-40; -55 °C	*RH* ramp	Cruise	No
2. UN ; 200nm	200 nm	--	--	--	-40; -55 °C	*RH* ramp	Cruise	No
3. UN ; 100nm	100 nm	--	--	--	-40; -55 °C	*RH* ramp	Cruise	No
4. UN ; Mixing state	400 nm	--	--	--	-40; -55 °C	*RH* ramp	Cruise	Yes
5. UN ; 100% thrust	400 nm	--	--	--	-40; -55 °C	*RH* ramp	100% thrust	No

6. CL ; 400nm	400 nm	-45 °C	104%	- 20 °C/<100 %	-40; -55 °C	*RH* ramp	Cruise	No
7. CL ; 200nm	200 nm	-45 °C	104%	-20 °C K/<100%	-40; -55 °C	*RH* ramp	Cruise	No
8. CL ; Pre-activation	400 nm	-45 °C	104%	20 °C K/<100%	-40; -55 °C	*RH* ramp	Cruise	No
9. CL ; 100nm	100 nm	-45 °C	104%	-20 °C K/<100%	-40; -55 °C	*RH* ramp	Cruise	No
10. CL ; Mixing state	400 nm	-45 °C	104%	-20 °C K/<100%	-40; -55 °C	*RH* ramp	Cruise	Yes
11. CL ; 100% thrust	400 nm	-45 °C	104%	-20 °C K/<100%	-40; -55 °C	*RH* ramp	100% thrust	No

Table 4: Experiment plan. Experiments 1 to 5: Unprocessed (UN) aircraft soot. Experiments 6 to 11: Cloud processed (CL) aircraft soot. Experiments 9 to 11 will depend on the results of experiments 3 to 5. A thermal denuder removing the volatile fraction of soot particles and added downstream of the ice nucleation chambers will allows to quantify the effect of mixing state. "*RH* ramp" means varying *RH* from RH_i = ~100% to RH_w slightly >100%, at a constant rate.

The experiments conducted at the airport will annex themselves to ongoing aircraft turbine engine tests and will depend, therefore, on the engine test schedule. Experiments 1 to 5 will be conducted from October to November 2021, while experiments 6 to 11 from April to May 2022.

4 Conclusions

The observational climatology of aviation aerosol, with its over 1100 unique aircraft plumes, is a solid basis for statistical analysis. Furthermore, the climatology covers the global main aviation corridors from Europe to North America, South Africa, and East Asia as well as all annual seasons. It is the first collection of aviation aerosol data that makes statistical analysis of the physical state of aged aviation aerosol within the atmosphere possible.

The first analysis could show that even the randomly observed and thereby already aged plume aerosol shows separate modes of soot (non-volatile) and sulphuric acid (volatile) particles.
Although, the number of the smaller and the larger aerosol particles were generally enhanced within the aircraft plumes compared to the background, the analysis of the accumulation mode fraction could additionally show that relatively more larger particles, with diameters > 250 nm like soot, were observed within the aircraft plume compared to the background aerosol.

In summary ice nucleation experiments involving turbine soot particles will be conducted in the next phase of the project. During this time, cloud processing experiments will be targeted from the turbine soot particles. Due to the large expense and limited sampling time of turbine soot particles, other ageing influences like exposure to ozone and organic condensation experiments will have to be performed with laboratory generated proxies of aviation soot particles. We have shown with some laboratory experiments that the extent of H_2SO_4 coating on the soot particles is important to determine the contribution of these particles to cirrus cloud formation. Furthermore, we have shown that large amounts of O_3 do not influence the soot ice nucleation ability at cirrus cloud relevant temperatures. One caveat to the above experiments is that the particles were exposed to O_3 under dark conditions. A different experiment that can be targeted is potential changes if the experiment is done under UV light representing the solar spectrum.

However, we aim to quantify the influence of volatile organic carbon emissions on the ice nucleation properties of turbine soot particles, by sampling the soot particles in the absence and presence of a catalytic stripper, which will be responsible for removing all the organic carbon from the turbine emissions. This will give us a clear indication of the role of VOCs on the cirrus forming properties of aviation soot.

5 Literature

Bescond, A., Yon, J., Ouf, F. X., Ferry, D., Delhaye, D., Gaffié, D., . . . Rozé, C. (2014). Automated Determination of Aggregate Primary Particle Size Distribution by TEM Image Analysis: Application to Soot. *Aerosol Science and Technology, 48*(8), 831-841. doi:10.1080/02786826.2014.932896

Bhandari, J., China, S., Chandrakar, K. K., Kinney, G., Cantrell, W., Shaw, R. A., . . . Mazzoleni, C. (2019). Extensive Soot Compaction by Cloud Processing from Laboratory and Field Observations. *Sci Rep, 9*(1), 11824. doi:10.1038/s41598-019-48143-y

Brooks, S. D., Suter, K., & Olivarez, L. (2014). Effects of Chemical Aging on the Ice Nucleation Activity of Soot and Polycyclic Aromatic Hydrocarbon Aerosols. *The Journal of Physical Chemistry A, 118*(43), 10036-10047. doi:10.1021/jp508809y

Browne, E. C., Franklin, J. P., Canagaratna, M. R., Massoli, P., Kirchstetter, T. W., Worsnop, D. R., . . . Kroll, J. H. (2014). Changes to the Chemical Composition of Soot from Heterogeneous Oxidation Reactions. *The Journal of Physical Chemistry A, 119*(7), 1154-1163. doi:10.1021/jp511507d

Bundke, U., Berg, M., Houben, N., Ibrahim, A., Fiebig, M., Tettich, F., . . . Petzold, A. (2015a). The IAGOS-CORE aerosol package: instrument design, operation and performance for continuous measurement aboard in-service aircraft. *Tellus B: Chemical and Physical Meteorology, 67*(1), 28339. doi:10.3402/tellusb.v67.28339

Bundke, U., Berg, M., Houben, N., Ibrahim, A., Fiebig, M., Tettich, F., . . . Petzold, A. (2015b). The IAGOS-CORE aerosol package: instrument design, operation and performance for continuous measurement aboard in-service aircraft. *Tellus B., 67*(1), 28339. doi:10.3402/tellusb.v67.28339

Burkhardt, U., Bock, L., & Bier, A. (2018). Mitigating the contrail cirrus climate impact by reducing aircraft soot number emissions. *npj Clim. Atmos. Sci., 1*(1), 37. doi:10.1038/s41612-018-0046-4

China, S., Kulkarni, G., Scarnato, B. V., Sharma, N., Pekour, M., Shilling, J. E., . . . Mazzoleni, C. (2015). Morphology of diesel soot residuals from supercooled water droplets and ice crystals: implications for optical properties. *Environmental Research Letters, 10*(11), 114010. doi:10.1088/1748-9326/10/11/114010

Christenson, H. K. (2013). Two-step crystal nucleation via capillary condensation. *CrystEngComm, 15*(11), 2030-2039. doi:10.1039/C3CE26887J

David, R. O., Marcolli, C., Fahrni, J., Qiu, Y., Perez Sirkin, Y. A., Molinero, V., . . . Kanji, Z. A. (2019). Pore condensation and freezing is responsible for ice formation below water saturation for porous particles. *Proceedings of the National Academy of Sciences, 116*(17), 8184-8189. doi:10.1073/pnas.1813647116

Delhaye, D., Ouf, F.-X., Ferry, D., Ortega, I. K., Penanhoat, O., Peillon, S., . . . Gaffie, D. (2017). The MERMOSE project: Characterization of particulate matter emissions of a commercial aircraft engine. *Journal of Aerosol Science, 105*, 48-63. doi:https://doi.org/10.1016/j.jaerosci.2016.11.018

Demott, P. J. (1990). An Exploratory-Study of Ice Nucleation by Soot Aerosols. *Journal of Applied Meteorology, 29*(10), 1072-1079. doi:Doi 10.1175/1520-0450(1990)029<1072:Aesoin>2.0.Co;2

DeMott, P. J., Chen, Y., Kreidenweis, S. M., Rogers, D. C., & Sherman, D. E. (1999). Ice formation by black carbon particles. *Geophysical Research Letters, 26*(16), 2429-2432. doi:Doi 10.1029/1999gl900580

Ess, M. N., & Vasilatou, K. (2019). Characterization of a new miniCAST with diffusion flame and premixed flame options: Generation of particles with high EC content in the size range 30 nm to 200 nm. *Aerosol Science and Technology, 53*(1), 29-44. doi:10.1080/02786826.2018.1536818

Finlayson-Pitts, B. J., & Pitts, J. N. (2000). CHAPTER 6 - Rates and Mechanisms of Gas-Phase Reactions in Irradiated Organic – NOx – Air Mixtures. In B. J. Finlayson-Pitts & J. N. Pitts (Eds.), *Chemistry of the Upper and Lower Atmosphere* (pp. 179-263). San Diego: Academic Press.

Friebel, F., Lobo, P., Neubauer, D., Lohmann, U., Drossaart van Dusseldorp, S., Mühlhofer, E., & Mensah, A. A. (2019). Impact of isolated atmospheric aging processes on the cloud condensation nuclei activation of soot particles. *Atmospheric Chemistry and Physics, 19*(24), 15545-15567. doi:10.5194/acp-19-15545-2019

Grimonprez, S., Faccinetto, A., Batut, S., Wu, J., Desgroux, P., & Petitprez, D. (2018). Cloud condensation nuclei from the activation with ozone of soot particles sampled from a kerosene diffusion flame. *Aerosol Science and Technology, 52*(8), 814-827. doi:10.1080/02786826.2018.1472367

Kanji, Z. A., Ladino, L. A., Wex, H., Boose, Y., Burkert-Kohn, M., Cziczo, D. J., & Kramer, M. (2017). Overview of Ice Nucleating Particles. In D. Baumgardner, G. M. McFarquhar, & A. J. Heymsfield (Eds.), *Ice Formation and Evolution in Clouds and Precipitation: Measurement and Modeling Challenges* (Vol. 58). Boston: Amer Meteorological Society.

Kanji, Z. A., Welti, A., Corbin, J. C., & Mensah, A. A. (2020). Black Carbon Particles Do Not Matter for Immersion Mode Ice Nucleation. *Geophysical Research Letters, 47*(11). doi:10.1029/2019gl086764

Kärcher, B. (2018). Formation and radiative forcing of contrail cirrus. *Nature Communications, 9*(1), 1824. doi:10.1038/s41467-018-04068-0

Kärcher, B., Mahrt, F., & Marcolli, C. (2021). Process-oriented analysis of aircraft soot-cirrus interactions constrains the climate impact of aviation. *Commun. Earth Environ., 2*(1), 113. doi:10.1038/s43247-021-00175-x

Koop, T., Luo, B., Tsias, A., & Peter, T. (2000). Water activity as the determinant for homogeneous ice nucleation in aqueous solutions. *Nature, 406*(6796), 611-614. doi:10.1038/35020537

Lacher, L., Lohmann, U., Boose, Y., Zipori, A., Herrmann, E., Bukowiecki, N., . . . Kanji, Z. A. (2017). The Horizontal Ice Nucleation Chamber (HINC): INP measurements at conditions relevant for mixed-phase clouds at the High Altitude Research Station Jungfraujoch. *Atmospheric Chemistry and Physics, 17*(24), 15199-15224. doi:10.5194/acp-17-15199-2017

Lee, D. S., Fahey, D. W., Skowron, A., Allen, M. R., Burkhardt, U., Chen, Q., . . . Wilcox, L. J. (2021). The contribution of global aviation to anthropogenic climate forcing for 2000 to 2018. *Atmospheric Environment, 244*, 117834. doi:https://doi.org/10.1016/j.atmosenv.2020.117834

Liati, A., Brem, B. T., Durdina, L., Vögtli, M., Arroyo Rojas Dasilva, Y., Dimopoulos Eggenschwiler, P., & Wang, J. (2014). Electron Microscopic Study of Soot Particulate Matter Emissions from Aircraft Turbine Engines. *Environmental Science & Technology, 48*(18), 10975-10983. doi:10.1021/es501809b

Liati, A., Schreiber, D., Alpert, P. A., Liao, Y., Brem, B. T., Corral Arroyo, P., . . . Dimopoulos Eggenschwiler, P. (2019). Aircraft soot from conventional fuels and biofuels during ground idle and climb-out conditions: Electron microscopy and X-ray micro-spectroscopy. *Environmental Pollution, 247*, 658-667. doi:https://doi.org/10.1016/j.envpol.2019.01.078

Lobo, P., Durdina, L., Smallwood, G. J., Rindlisbacher, T., Siegerist, F., Black, E. A., . . . Wang, J. (2015). Measurement of Aircraft Engine Non-Volatile PM Emissions: Results of the Aviation-Particle Regulatory Instrumentation Demonstration Experiment (A-PRIDE) 4 Campaign. *Aerosol Science and Technology, 49*(7), 472-484. doi:10.1080/02786826.2015.1047012

Lupi, L., & Molinero, V. (2014). Does Hydrophilicity of Carbon Particles Improve Their Ice Nucleation Ability? *The Journal of Physical Chemistry A, 118*(35), 7330-7337. doi:10.1021/jp4118375

Ma, X., Zangmeister, C. D., Gigault, J., Mulholland, G. W., & Zachariah, M. R. (2013). Soot aggregate restructuring during water processing. *Journal of Aerosol Science, 66*, 209-219. doi:https://doi.org/10.1016/j.jaerosci.2013.08.001

Mahrt, F., Alpert, P. A., Dou, J., Gronquist, P., Arroyo, P. C., Ammann, M., . . . Kanji, Z. A. (2020b). Aging induced changes in ice nucleation activity of combustion aerosol as determined by near edge X-ray absorption fine structure (NEXAFS) spectroscopy. *Environ Sci Process Impacts, 22*(4), 895-907. doi:10.1039/c9em00525k

Mahrt, F., Kilchhofer, K., Marcolli, C., Grönquist, P., David, R. O., Rösch, M., . . . Kanji, Z. A. (2020a). The Impact of Cloud Processing on the Ice Nucleation Abilities of Soot Particles at Cirrus Temperatures. *Journal of Geophysical Research: Atmospheres, 125*(3). doi:10.1029/2019jd030922

Mahrt, F., Marcolli, C., David, R. O., Grönquist, P., Barthazy Meier, E. J., Lohmann, U., & Kanji, Z. A. (2018). Ice nucleation abilities of soot particles determined with the Horizontal Ice Nucleation Chamber. *Atmospheric Chemistry and Physics, 18*(18), 13363-13392. doi:10.5194/acp-18-13363-2018

Marcolli, C. (2014). Deposition nucleation viewed as homogeneous or immersion freezing in pores and cavities. *Atmospheric Chemistry and Physics, 14*(4), 2071-2104. doi:10.5194/acp-14-2071-2014

Marcolli, C. (2020). Technical note: Fundamental aspects of ice nucleation via pore condensation and freezing including Laplace pressure and growth into macroscopic ice. *Atmospheric Chemistry and Physics, 20*(5), 3209-3230. doi:10.5194/acp-20-3209-2020

Marcolli, C., Mahrt, F., & Kärcher, B. (2021). Soot-PCF: Pore condensation and freezing framework for soot aggregates. *Atmos. Chem. Phys. Discuss., 2020*, 1-68. doi:10.5194/acp-2020-1134

Marhaba, I., Ferry, D., Laffon, C., Regier, T. Z., Ouf, F.-X., & Parent, P. (2019). Aircraft and MiniCAST soot at the nanoscale. *Combustion and Flame, 204*, 278-289. doi:https://doi.org/10.1016/j.combustflame.2019.03.018

Miake-Lye R. C., Martinez-Sanchez M., Brown R. C., & E., K. C. (1993). Plume and wake dynamics, mixing, and chemistry behind a high speed civil transport aircraft. *Journal of Aircraft, 30*(4), 467-479. doi:10.2514/3.46368

Möhler, O., Büttner, S., Linke, C., Schnaiter, M., Saathoff, H., Stetzer, O., . . . Schurath, U. (2005). Effect of sulfuric acid coating on heterogeneous ice nucleation by soot aerosol particles. *Journal of Geophysical Research: Atmospheres, 110*(D11). doi:https://doi.org/10.1029/2004JD005169

Mohler, O., Linke, C., Saathoff, H., Schnaiter, M., Wagner, R., Mangold, A., . . . Schurath, U. (2005). Ice nucleation on flame soot aerosol of different organic carbon content. *Meteorologische Zeitschrift, 14*(4), 477-484. doi:10.1127/0941-2948/2005/0055

Moore, R. H., Thornhill, K. L., Weinzierl, B., Sauer, D., D'Ascoli, E., Kim, J., . . . Anderson, B. E. (2017). Biofuel blending reduces particle emissions from aircraft engines at cruise conditions. *Nature, 543*(7645), 411-415. doi:10.1038/nature21420

Murphy, D. M., & Koop, T. (2005). Review of the vapour pressures of ice and supercooled water for atmospheric applications. *Quarterly Journal of the Royal Meteorological Society, 131*(608), 1539-1565. doi:https://doi.org/10.1256/qj.04.94

Murray, B. J., O'Sullivan, D., Atkinson, J. D., & Webb, M. E. (2012). Ice nucleation by particles immersed in supercooled cloud droplets. *Chem Soc Rev, 41*(19), 6519-6554. doi:10.1039/c2cs35200a

Nichman, L., Wolf, M., Davidovits, P., Onasch, T. B., Zhang, Y., Worsnop, D. R., . . . Cziczo, D. J. (2019). Laboratory study of the heterogeneous ice nucleation on black-carbon-containing aerosol. *Atmospheric Chemistry and Physics, 19*(19), 12175-12194. doi:10.5194/acp-19-12175-2019

Petzold, A., Busen, R., Schröder, F. P., Baumann, R., Kuhn, M., Ström, J., . . . Schumann, U. (1997). Near-field measurements on contrail properties from fuels with different sulfur content. *Journal of Geophysical Research: Atmospheres, 102*(D25), 29867-29880. doi:https://doi.org/10.1029/97JD02209

Petzold, A., Döpelheuer, A., Brock, C. A., & F., S. (1999). In situ observations and model calculations of black carbon emission by aircraft at cruise altitude. *Journal of Geophysical Research: Atmospheres, 104*(D18), 22171-22181. doi:https://doi.org/10.1029/1999JD900460

Petzold, A., Fiebig, M., Fritzsche, L., Stein, C., Schumann, U., Wilson, C. W., . . . Hughes, K. (2005a). Particle emissions from aircraft engines a survey of the European project PartEmis. *Meteorol. Z., 14*, 465-476. doi:10.1127/0941-2948/2005/0054

Petzold, A., Gysel, M., Vancassel, X., Hitzenberger, R., Puxbaum, H., Vrochticky, S., . . . Mirabel, P. (2005b). On the effects of organic matter and sulphur-containing compounds on the CCN activation of combustion particles. *Atmospheric Chemistry and Physics, 5*(12), 3187-3203. doi:10.5194/acp-5-3187-2005

Petzold, A., Ogren, J. A., Fiebig, M., Laj, P., Li, S. M., Baltensperger, U., . . . Zhang, X. Y. (2013). Recommendations for reporting "black carbon" measurements. *Atmospheric Chemistry and Physics, 13*(16), 8365-8379. doi:10.5194/acp-13-8365-2013

Petzold, A., Stein, C., Nyeki, S., Gysel, M., Weingartner, E., Baltensperger, U., . . . Wilson, C. W. (2003). Properties of jet engine combustion particles during the PartEmis experiment: Microphysics and Chemistry. *Geophys. Res. Lett., 30*(13). doi:10.1029/2003GL017283

Petzold, A., Strom, J., Ohlsson, S., & Schroder, F. P. (1998). Elemental composition and morphology of ice-crystal residual particles in cirrus clouds and contrails. *Atmospheric Research, 49*(1), 21-34. doi:Doi 10.1016/S0169-8095(97)00083-5

Popovicheva, O., Kireeva, E., Persiantseva, N., Khokhlova, T., Shonija, N., Tishkova, V., & Demirdjian, B. (2008). Effect of soot on immersion freezing of water and possible atmospheric implications. *Atmospheric Research, 90*(2), 326-337. doi:https://doi.org/10.1016/j.atmosres.2008.08.004

Popovicheva, O. B., Persiantseva, N. M., Kireeva, E. D., Khokhlova, T. D., & Shonija, N. K. (2011). Quantification of the Hygroscopic Effect of Soot Aging in the Atmosphere: Laboratory Simulations. *The Journal of Physical Chemistry A, 115*(3), 298-306. doi:10.1021/jp109238x

Popovicheva, O. B., Persiantseva, N. M., Lukhovitskaya, E. E., Shonija, N. K., Zubareva, N. A., Demirdjian, B., . . . Suzanne, J. (2004). Aircraft engine soot as contrail nuclei. *Geophysical Research Letters, 31*(11). doi:https://doi.org/10.1029/2003GL018888

Pósfai, M., Anderson, J. R., Buseck, P. R., & Sievering, H. (1999). Soot and sulfate aerosol particles in the remote marine troposphere. *Journal of Geophysical Research: Atmospheres, 104*(D17), 21685-21693. doi:10.1029/1999jd900208

Righi, M., Hendricks, J., & Beer, C. G. (2021). Exploring the uncertainties in the aviation soot-cirrus effect. *Atmos. Chem. Phys. Discuss., 2021*, 1-31. doi:10.5194/acp-2021-329

Schröder, F., Brock, C. A., Baumann, R., Petzold, A., Busen, R., Schulte, P., & Fiebig, M. (2000). In situ studies on volatile jet exhaust particle emissions: Impact of fuel sulfur content and environmental conditions on nuclei mode aerosols. *J. Geophys. Res.-Atmos., 105*(D15), 19941-19954. doi:10.1029/2000JD900112

Schumann, U., Arnold, F., Busen, R., Curtius, J., Kärcher, B., Kiendler, A., . . . Wohlfrom, K.-H. (2002). Influence of fuel sulfur on the composition of aircraft exhaust plumes: The experiments SULFUR 1–7. *Journal of Geophysical Research: Atmospheres, 107*(D15), AAC 2-1-AAC 2-27. doi:https://doi.org/10.1029/2001JD000813

Stratmann, G., Ziereis, H., Stock, P., Brenninkmeijer, C. A. M., Zahn, A., Rauthe-Schöch, A., . . . Volz-Thomas, A. (2016a). NO and NOy in the upper troposphere: Nine years of CARIBIC measurements onboard a passenger aircraft. *Atmospheric Environment, 133*, 93-111. doi:https://doi.org/10.1016/j.atmosenv.2016.02.035

Stratmann, G., Ziereis, H., Stock, P., Brenninkmeijer, C. A. M., Zahn, A., Rauthe-Schöch, A., . . . Volz-Thomas, A. (2016b). NO and NOy in the upper troposphere: Nine years of CARIBIC measurements onboard a passenger aircraft. *Atmos. Environ., 133*, 93-111. doi:10.1016/j.atmosenv.2016.02.035

Suzanne J, Ferry D, Popovitcheva O, & K Shonija N K. (2003). Ice nucleation by kerosene soot under upper tropospheric conditions. *Canadian Journal of Physics, 81*(1-2), 423-429. doi:10.1139/p03-004

Twohy, C. H., & Gandrud, B. W. (1998). Electron microscope analysis of residual particles from aircraft contrails. *Geophysical Research Letters, 25*(9), 1359-1362. doi:10.1029/97gl03162

Twohy, C. H., & Poellot, M. R. (2005). Chemical characteristics of ice residual nuclei in anvil cirrus clouds: evidence for homogeneous and heterogeneous ice formation. *Atmospheric Chemistry and Physics, 5*, 2289-2297. doi:DOI 10.5194/acp-5-2289-2005

Ullrich, R., Hoose, C., Möhler, O., Niemand, M., Wagner, R., Höhler, K., . . . Leisner, T. (2017). A New Ice Nucleation Active Site Parameterization for Desert Dust and Soot. *Journal of the Atmospheric Sciences, 74*(3), 699-717. doi:10.1175/jas-d-16-0074.1

Vali, G., DeMott, P. J., Möhler, O., & Whale, T. F. (2015). Technical Note: A proposal for ice nucleation terminology. *Atmospheric Chemistry and Physics, 15*(18), 10263-10270. doi:10.5194/acp-15-10263-2015

Vander Wal, R. L., Bryg, V. M., & Hays, M. D. (2010). Fingerprinting soot (towards source identification): Physical structure and chemical composition. *Journal of Aerosol Science, 41*(1), 108-117. doi:https://doi.org/10.1016/j.jaerosci.2009.08.008

Wentzel, M., Gorzawski, H., Naumann, K. H., Saathoff, H., & Weinbruch, S. (2003). Transmission electron microscopical and aerosol dynamical characterization of soot aerosols. *Journal of Aerosol Science, 34*(10), 1347-1370. doi:https://doi.org/10.1016/S0021-8502(03)00360-4

Zhang, C., Zhang, Y., Wolf, M. J., Nichman, L., Shen, C., Onasch, T. B., . . . Cziczo, D. J. (2020). The effects of morphology, mobility size, and secondary organic aerosol (SOA) material coating on the ice nucleation activity of black carbon in the cirrus regime. *Atmospheric Chemistry and Physics, 20*(22), 13957-13984. doi:10.5194/acp-20-13957-2020

Zhang, R., Khalizov, A. F., Pagels, J., Zhang, D., Xue, H., & McMurry, P. H. (2008). Variability in morphology, hygroscopicity, and optical properties of soot aerosols during atmospheric processing. *Proceedings of the National Academy of Sciences, 105*(30), 10291-10296. doi:10.1073/pnas.0804860105